Nano Energy 45 (2018) 346–352

Contents lists available at ScienceDirect

Nano Energy

journal homepage: www.elsevier.com/locate/nanoen

Full paper

Flexible ReS_2 nanosheets/N-doped carbon nanofibers-based paper as a universal anode for alkali (Li, Na, K) ion battery

Minglei Mao[a,b], Chunyu Cui[b], Mingguang Wu[b], Ming Zhang[b], Tao Gao[a], Xiulin Fan[a], Ji Chen[a], Taihong Wang[b], Jianmin Ma[b], Chunsheng Wang[a,*]

[a] Department of Chemical and Biomolecular Engineering, University of Maryland, College Park, MD 20742, United States
[b] School of Physics and Electronics, Hunan University, Changsha 410082, China

ARTICLE INFO

Keywords:
Universal anode
ReS_2
N-doped carbon nanofibers
Alkali (Li, Na, and K) ion battery

ABSTRACT

Alkali (Li, Na, K) ion battery have practically or potentially been widely used as a power source for portable electronic devices and electric vehicles. However, lack of universal anodes for these three alkali ion battery are restricting their development, especially for Na-ion battery and K-ion battery. Rhenium disulfide (ReS_2), with large interlayer space and weak van der Waals interaction between layers, can afford massive alkali (lithium, sodium, and potassium) ions to diffuse easily between the layers. However, its low electronic conductivity and large volume changes in the conversion reaction significantly compromise the cycle life. To address this issue, here, we anchor ReS_2 nanosheets onto nitrogen doped carbon nanofibers (N-CNF) which forms a flexible ReS_2/N-CNFs paper for alkali (Li, Na, and K) ion battery anodes. The carbon nanofibers (CNFs) can improve the conductivity and the doped nitrogen can absorb sulfur and polysulfide generated by the conversion reaction. As a result, the ReS_2/N-CNFs composite anode maintains a reversible capacity of 430 mAh/g after 400 cycles at 100 mA/g in LIBs, 245 mAh/g after 800 cycles at 100 mA/g in NIBs, and 253 mAh/g after 100 cycles at 50 mA/g in KIBs. This performance is one of the best among all ReS_2 reported up to date. In addition, the solid electrolyte interface formation on ReS_2 and the coulombic efficiency in different alkali ion batteries are also systemically investigated.

1. Introduction

Because of the high energy density and long cycle life, lithium ion batteries (LIBs) have been widely used in portable electronics and power electric vehicles (EVs) [1–3]. Nevertheless, the currently commercialized LIBs cannot meet the growing demand for these electronic devices on energy and power. Due to the limited lithium supply, sodium ion batteries (NIBs) have attracted intensive interests as an alternative to LIBs for applications where cost is an important factor [4,5]. Nevertheless, the energy density of NIB is lower than that of LIB due to relatively high standard potential of sodium (−2.71 V vs. E°) compared to lithium (−3.04 V vs. E°) [6,7]. Another promising alternative for low cost application is potassium ion batteries (KIBs) due to natural abundance and suitable potential (−2.93 V vs. E°) closed to lithium [8–10]. These three alkali ion batteries are complementary and suitable for different applications. Over the past two decades, graphite has been the most widely used anode for LIBs. However, graphite suffers from low capacity and poor rate performance as Li-ion battery anodes (372 mAh/g) [3,11,12], and it is not suitable for NIB anodes [13], and also has a low capacity for KIBs (279 mAh/g) [14,15]. Thus, exploring a universal high capacity electrode material that is suitable for these three alkali ion batteries are of practical importance.

2D transition metal dichalcogenides (TMDs) compounds that are composed of group VI transition metals (Mo, W, or Re) and chalcogens (S or Se) have received surging research interests as anode candidates for alkali ion batteries [16–20]. Rhenium disulfide (ReS_2), as a new member of TMDs family, have inherent anisotropy and much weaker interlayer coupling resulting from additional valence electron in rhenium [21–23]. As the anode material for LIB, it has a theoretical capacity of 430 mAh/g due to its 4-electron transfer reaction [16,24,25]. In addition, ReS_2 possesses much less coupling energy (~18 meV per unit cell) compared to MoS_2 (~460 meV) [26], although their interlayer spacing are comparative (6.14 Å for ReS_2 and 6.15 Å for MoS_2) (Fig. S1a, b) [16]. The large interlayer spacing and extremely weak van der Waals attraction between layers allow the facile diffusion of alkali metal ions within layers. This feature enables ReS_2 to be a natural candidate as a universal anode material for all alkali ion batteries. However, the low conductivity and poor cycling performance of ReS_2

* Corresponding author.
E-mail addresses: nanoelechem@hnu.edu.cn (J. Ma), cswang@umd.edu (C. Wang).

https://doi.org/10.1016/j.nanoen.2018.01.001
Received 16 November 2017; Received in revised form 28 December 2017; Accepted 1 January 2018
Available online 02 January 2018

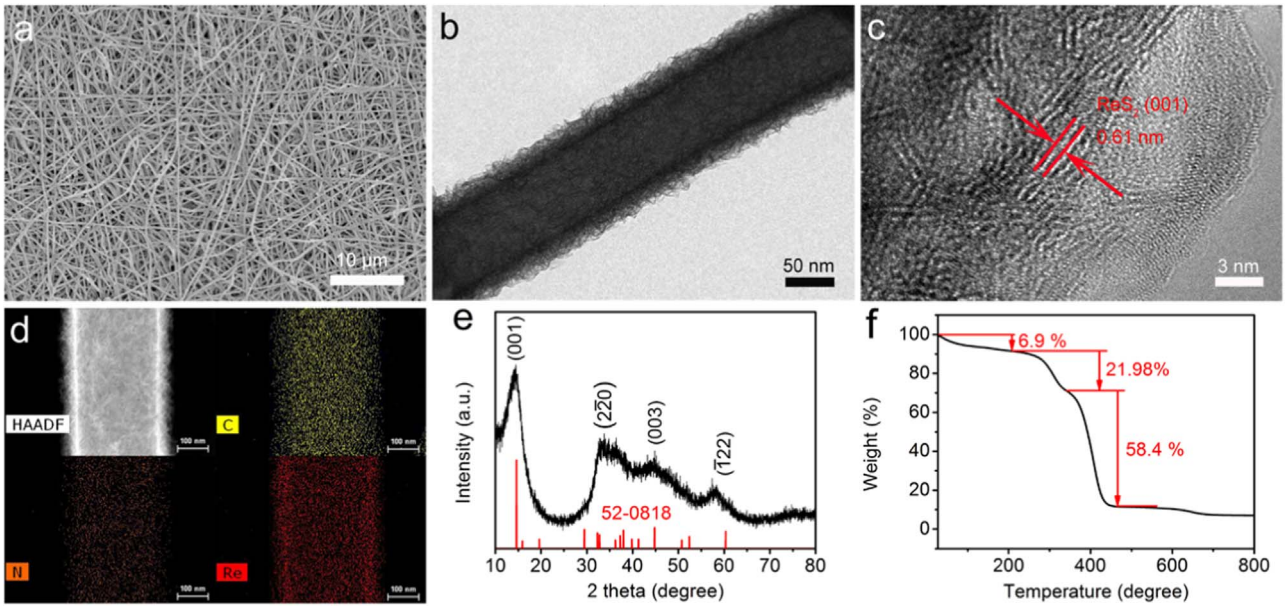

Fig. 1. (a) SEM of ReS_2/N-CNFs. (b) TEM and (c) HR-TEM images of ReS_2/N-CNFs. (d) TEM observation and corresponding EDS elemental mapping of carbon, nitrogen, and rhenium. (e) XRD pattern and (f) TGA curve of ReS_2/N-CNFs in air at a rate of 5 °C/min.

severely restrict its application in batteries [27,28]. Despite the conductivity of ReS_2 can be enhanced by mixing with carbon conductive network [28–30], capacity fading has not been resolved, because Li_2S_x produced by the conversion reaction of ReS_2 during cycling dissolve in the electrolyte and cause active materials loss.

Herein, we proposed a novel ReS_2 composites to solve the aforementioned low conductivity and polysulfide dissolution problem simultaneously. The ReS_2 nanosheets is anchored on N-doped carbon nanofibers (ReS_2/N-CNFs) with a facile electrospinning and hydrothermal method, which not only provides electronic conductivity but also offer chemical adsorption to the formed polysulfide. Combining all the advantages of the composite anode (the large interlayer spacing and extremely weakly van der Waals interaction of ReS_2, high conductivity, oriented electronic/ionic transport pathway of CNFs, and strong absorption of nitrogen doping to sulfur and polysulfide) [31,32], the ReS_2/N-CNFs-based paper show outstanding electrochemical performance in LIBs, NIBs, and KIBs, demonstrating its supremacy as a universal anode materials for these alkali ion batteries.

2. Experimental section

2.1. Preparation of ReS_2/N-CNFs

0.43 g polyacrylonitrile (PAN) was added into 6 mL N, N-dimethyl formamide and stirred for 2 h in 60 °C to obtain the transparent solution. Then, the precursor solution was transferred into a 20 mL syringe with a stainless steel needle (with 0.71 mm inner diameter). A syringe pump controlled the flow rate to about 0.2 mL/h. A piece of aluminum foil used as the collector was vertically positioned about 15 cm away from the needle. A high voltage DC power supple of 11–14 kV between needle and aluminum foil was obtained. After pre-oxidation of the obtained nanofibers at 230 °C in air for 6 h, the brown mats were treated at 720 °C in argon for 2 h to get the N-doped CNFs [33].

66 mg NH_4ReO_4 and 120 mg thioacetamide (C_2H_5NS) were dissolved in 40 mL H_2O. After stirring for 10 min, 0.2 g hexamethylenetetramine was added to form a transparent solution. Then, 40 mg N-doped CNFs was immersed in the above solution. The solution was transferred into a Teflon-lined autoclave and maintained at 220 °C for 48 h. After cooling to room temperature, ReS_2/N-CNFs was rinsed with distilled water and ethanol for several time, and dried in a vacuum oven at 60 °C overnight. For comparison, pure ReS_2 was prepared under the same condition without the presence of N-doped CNFs.

2.2. Material Characterizations

Field emission scanning electron microscopy (FESEM, Model JSM-7600F, JEOL Ltd., Tokyo, Japan) was used to characterize the morphologies and size of the synthesized samples. The chemical composition was investigated by the energy dispersive X-ray spectroscopy (EDS). High resolution transmission electron microscopy (HRTEM) images were carried out with a JOEL JEM 2100F microscope. X-ray powder diffraction (XRD) patterns were recorded on a Bruke D8 Advance powder X-ray diffractometer with Cu Kα (λ = 0.15406 nm). X-ray photoelectron spectroscopy (XPS) was performed using an ESCALAB 250. Thermogravimetric analysis (TGA) was measured from 30 to 800 °C at a heating rate of 5 °C/min under 100 mL/min of flowing air with a Perkin-Elmer TGA 4000.

2.3. Electrochemical measurements

The final ReS_2/N-CNFs was cut into pieces with size of 5 × 5 mm^2 and directly used as anodes, each of which weigh ~1 mg. Electrochemical performance was tested in CR2032 coin cells, which were assembled in an argon-filled glove box with lithium, sodium, and potassium foil as the counter electrode, 1 M bis(trifluoromethane) sulfonamide lithium salt (LiTFSI, Sigma Aldrich) in a mixture of 1,3-dioxolane (DOL) and 1,2-dimethoxyethane (DME) (v/v, 1:1), 1 M NaSO3CF3 in diglyme, and 0.8 M KTFSI in DME as the electrolyte, respectively, and Celgard 2400 microporous polypropylene membrane as separators. Electrochemical performance was tested using an Arbin battery test station (BT2000, Arbin Instruments, USA) at various current rates with voltage cutoff of 0.01–3 V. Capacity was calculated on the basis of total mass of the entire ReS_2/N-CNFs. CV curves were recorded at a scan rate of 0.1 mV/s using an electrochemical work station. Nyquist plots were recorded using a Zahner IM6 electrochemical work station at a frequency range of 0.01–100 kHz.

3. Results and discussion

As shown in the scanning electron microscope (SEM) images in

Fig. 1a and Fig. S2a, the flexible ReS_2/N-CNFs paper consists of uniform straight nanofibers with a diameter of 200–400 nm. The interconnected conductive N-doped CNFs network favors fast electronic transportation. Such long fiber and interconnected structure ensure the excellent mechanical property (Fig. S3) and stability of ReS_2/N-CNFs paper during electrochemical processes. Whereas, pure ReS_2 forms anomalous spheres with diameter up to micrometer (Fig. S2b), which will cause slow kinetics for ions to diffuse into. Consistent with SEM results, a low-resolution TEM image (Fig. 1b) shows that ReS_2 nanosheets evenly anchor on the surface of N-doped CNFs with the diameter of ~200 nm. The specific surface area of ReS_2/N-CNFs is ~95.21 m^2/g by BET (Fig. S2c). From the high-resolution TEM (HR-TEM) image (Fig. 1c), (001) crystal facet of ReS_2 with layer space of 0.61 nm can be clearly observed. Besides, the energy dispersive X-ray spectroscopy (EDS) elemental mapping images (Fig. 1d) well match results shown in Fig. 1b. It is shown that nitrogen is evenly doped in the CNFs, while rhenium and sulfur constitute ReS_2 uniformly anchored on the surface of N-doped CNFs.

The structure and composition of ReS_2/N-CNFs are characterized by X-ray diffraction (XRD) and thermogravimetric analysis (TGA), respectively. As shown in Fig. 1e, all the main peaks in the pattern can be indexed to ReS_2 (JCPDS card No. 52-0818). No peaks for graphite is present, suggesting that carbon exists in amorphous state due to low calcination temperature [33]. The mass loading of ReS_2 in ReS_2/N-CNFs was measured using TGA (Fig. 1f). A mass loss of ~6.9% below 150 °C could be attributed to the loss of physically absorbed water. The weight loss of 21.98% at around 200–350 °C can be ascribed to the oxidation of ReS_2, corresponding to 23.75% of ReS_2 in ReS_2/N-CNFs. Moreover, an obvious weight loss of 58.4% arises from 350 to 480 °C, which can be ascribed to the oxidation of N-doped CNFs [34]. In addition, components of ReS_2/N-CNFs can be further confirmed by energy-dispersive spectrometry (EDS) in Fig. S4a.

X-ray photoelectron spectroscopy (XPS) was conducted to identify the chemical status of elements in ReS_2/N-CNFs (Fig. 2). Fig. 2a shows XPS survey spectra of ReS_2/N-CNFs, from which peaks of C 1s, N 1s, and Re 4f can be clearly observed. Fig. 2b exhibits a high-resolution C 1s XPS spectrum of ReS_2/N-CNFs. Two peaks centered at 284.8 and 286.1 eV can be assigned to extensively delocalized sp2-hybridized carbon atoms and the carbon-nitrogen bond, respectively [35,36]. The high-resolution N 1s XPS spectrum can be assigned to a pyrrolic nitrogen (a trigonal nitrogen phase bonded to a sp2-coordinated carbon) with binding energy of 401.0 eV and a classic graphitic-type quaternary nitrogen with binding energy of 402.3 eV (Fig. 2c) [37,38]. The N content in N-CNFs is ~11 at%. The high-resolution Re 4f XPS spectrum of ReS_2/N-CNFs exhibit two peaks at 42.7 and 45.1 eV, which can be attributed to the Re 4f7/2 and Re 4f5/2 spin orbit peaks of ReS_2, respectively (Fig. 2d). In addition, two S2p peaks at 163.2 and 164.3 eV further confirm the presence of ReS_2 (Fig. S4b). The XPS results corroborate the existence of ReS_2 and N-doped CNFs, which agrees well with the XRD results.

The electrochemical performance of ReS_2/N-CNFs anode in Li-ion batteries was evaluated in coin-type cells by directly using flexible ReS_2/N-CNFs paper as working electrodes and Li metal as a counter electrode (Fig. 3). Cyclic voltammetry (CV) curves of ReS_2/N-CNFs were conducted at the scan rate of 0.1 mV/s between 0.01 and 3 V (Fig. 3a). In the first cathodic scan, two dominant reduction peaks at ~1.32 and 0.71 V can be clearly seen. The peak at 1.32 V is ascribed to insertion of Li^+ into the layer space of ReS_2 to form Li_xReS_2 according to the reaction (1) [28,29,39]. The followed wide peak centered at 0.71 V is due to the formation of SEI and the reduction of Li_xReS_2 to Li_2S and metallic Re by a conversion reaction according to the reaction (2) [29,39]. In the following anodic scan, a peak centered at 1.83 V is associated with the delithiation of Li_2S + Re composite into Li_xReS_2, followed by a distinct peak located at 2.33 V which is contributed by the formation of ReS_2 [29,40].

$$\mathrm{Re}\,S_2 + xLi^+ + xe^- \rightarrow Li_x\,\mathrm{Re}\,S_2 \quad (1)$$

$$\mathrm{Li}_x\,\mathrm{Re}\,\mathrm{S}_2 + (4-x)Li^+ + (4-x)e^- \rightarrow \mathrm{Re} + 2Li_2S \quad (2)$$

During the 2nd and 3rd cycle, the reduction peaks at 1.32 V and 0.71 V shift to ~2 V and 1.23 V due to relaxation of stress and strain in

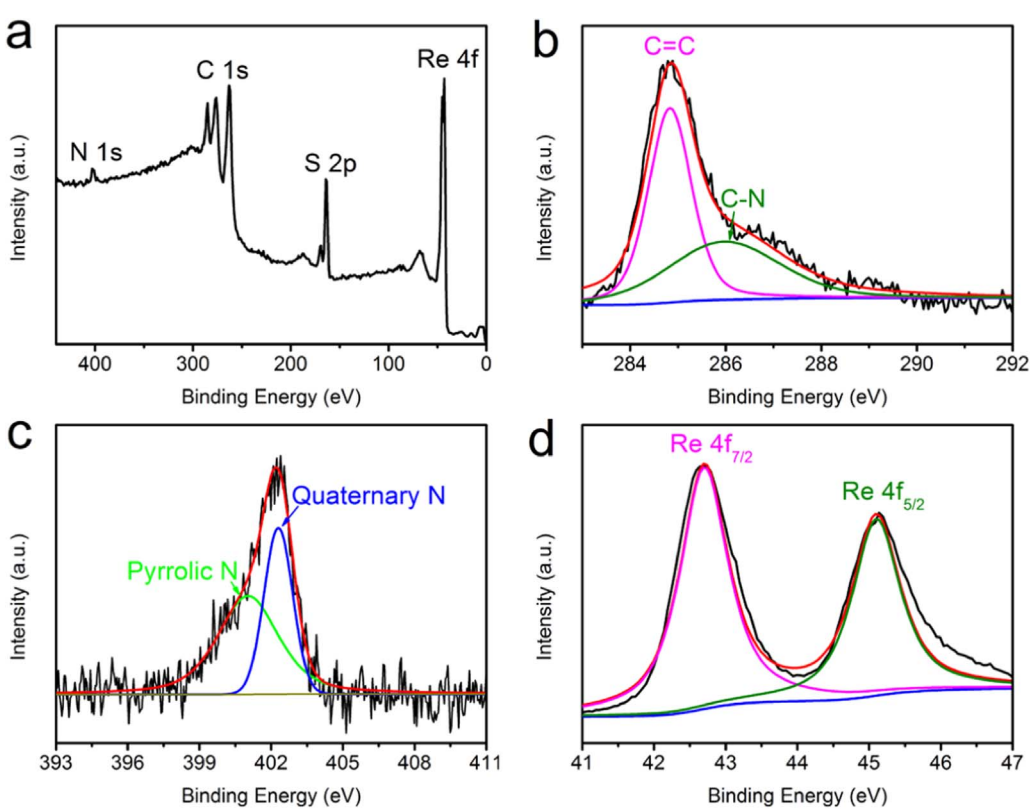

Fig. 2. (a) Survey XPS spectra of ReS_2/N-CNFs. (b-d) High-resolution XPS spectra of C 1s, N 1s, and Re 4f, respectively.

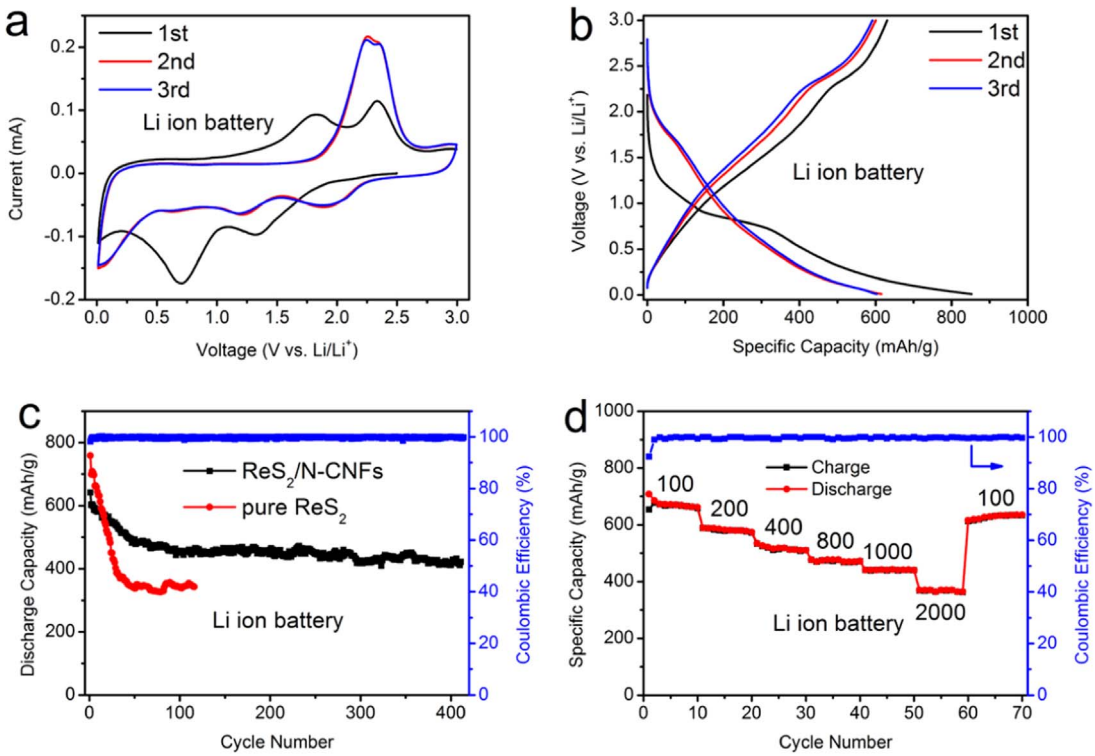

Fig. 3. Electrochemical performance of ReS_2/N-CNFs as a Li-ion battery anode.(a) Cyclic voltammetry curves of ReS_2/N-CNFs at a scan rate of 0.1 mV/s. (b) Galvanostatic discharge-charge profiles of ReS_2/N-CNFs for the first three cycles at a current density of 100 mA/g. (c) Cycling performance of the electrodes based on ReS_2/N-CNFs and pure ReS_2 at a current density of 100 mA/g. (d) Rate performance of ReS_2/N-CNFs at different current density (mA/g). The capacity of ReS_2/N-CNFs is based on the mass of entire electrodes.

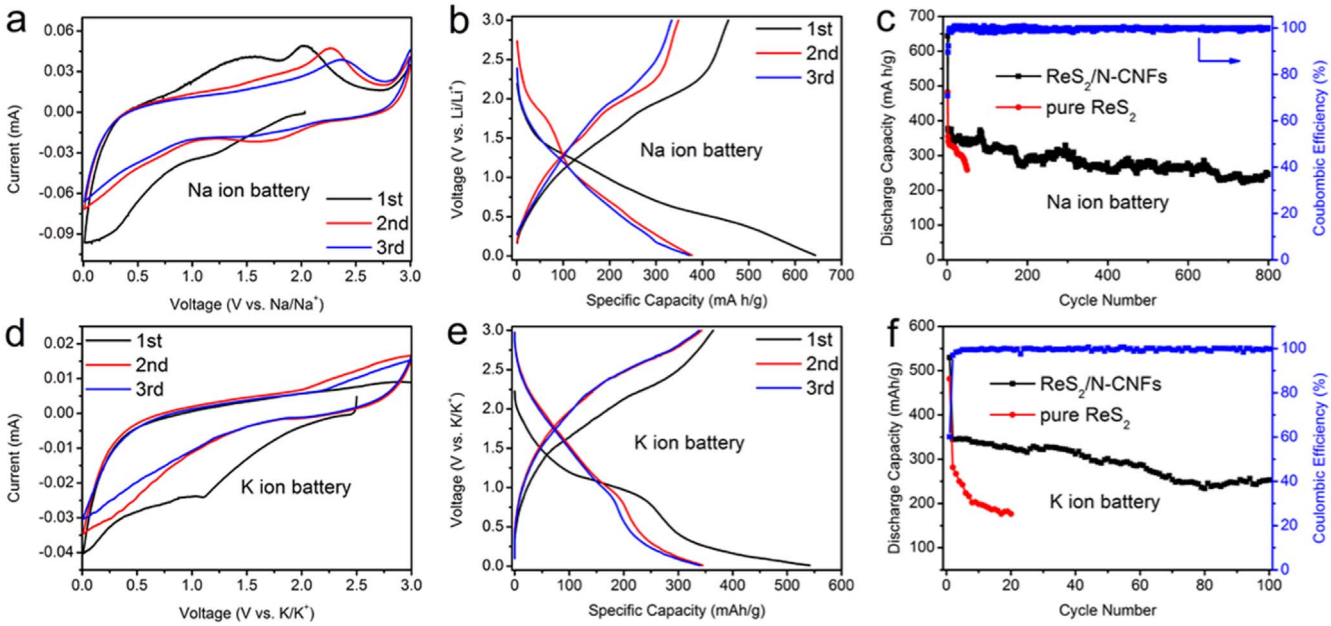

Fig. 4. Electrochemical performance of ReS_2/N-CNFs anode in Na-ion and K-ion batteries. (a-c) Cyclic voltammetry curves, galvanostatic discharge-charge profiles, and cycling performance of ReS_2/N-CNFs in NIBs, respectively. (d-f) Cyclic voltammetry curves, galvanostatic discharge-charge profiles, and cycling performance of ReS_2/N-CNFs in KIBs, respectively. The capacity of ReS_2/N-CNFs is based on the mass of entire electrodes.

the first charge/discharge cycle, while the delithiation of Li_2S+Re composite at 1.83 V also shift and merge with delithiation peak of Li_xReS_2 at 2.33 V.

The Galvanostatic discharge and charge curves of ReS_2/N-CNFs in LIBs in the first three cycles at a current density of 100 mA/g between 0.01 and 3 V are shown in Fig. 3b. There are two main plateau in the first discharge and charge curves, which is in accordance with the CV profiles. The first discharge and charge capacities of ReS_2/N-CNFs are 852 and 630 mAh/g, corresponding to the Coulombic Efficiency (CE) of 73.9%. The irreversible capacity can be mainly ascribed to the inevitable decomposition of electrolyte to form solid-electrolyte interphase (SEI) and irreversible conversion reaction in the first cycle [33,41]. The overlap of discharge and charge curves in the following two cycles implies the high cycling stability of ReS_2/N-CNFs.

The cycling performance of ReS_2/N-CNFs was evaluated at a current density of 100 mA/g (Fig. 3c). ReS_2/N-CNFs show a high capacity

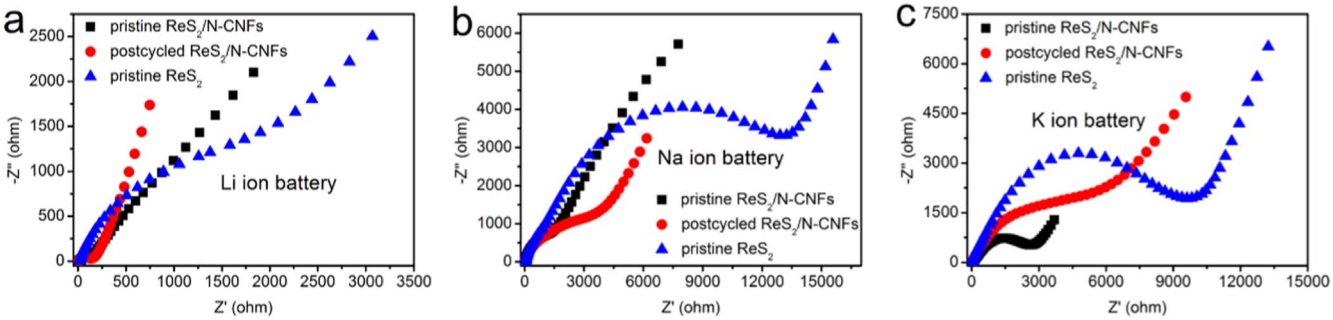

Fig. 5. (a-c) Nyquist plot of ReS_2/N-CNFs and pure ReS_2 before and after 100 cycles in LIBs, NIBs, and KIBs, respectively.

retention and good cycling stability, which can be attributed to the high conductivity of flexible N-doped CNFs paper and the strong absorption of nitrogen doping to lithium polysulfide. Even after 400 cycles, the reversible capacity of ReS_2/N-CNFs can be kept at 440 mA h/g after initial drop, which is more stable than ReS_2-based anodes previously reported (Table S1). In addition, the CE of ReS_2/N-CNFs maintains beyond 99.5% after the first 10 cycles, which is indicative of good cycling stability. In contrast, the capacity of pure ReS_2 quickly drops to around 340 mA h/g within 50 cycles, highlighting the contribution of N-doped CNFs to excellent cycling performance. Also, the cycling performance of N-CNFs for LIBs is conducted, which delivers the capacity of 232 mA h/g after 100 cycles (Fig. S4c). The rate performance of the as-synthesized ReS_2/N-CNFs in LIBs is shown in Fig. 3d. At a low current density of 100 mA/g, ReS_2/N-CNFs delivers a high discharge capacity of 660 mA h/g. When the current densities gradually increase from 200, 400, 800, 1000, to 2000 mA/g, corresponding capacities can maintain 580, 520, 470, 440, and 360 mA h/g, respectively. Then the capacity can recover to 630 mA h/g, when the current density is reduced to 100 mA/g. The results demonstrate that ReS_2/N-CNFs-based paper is a promising anode candidate for LIBs.

The sodium- and potassium-storage performances of ReS_2/N-CNFs were also evaluated in coin cells (Fig. 4). CV of ReS_2/N-CNFs for NIBs was conducted at a scan rate of 0.1 mV/s between 0.01 and 3 V (Fig. 4a). In the first cathodic scan, two peaks at 1.2 and 0.3 V can be attributed to insertion of Na^+ into the interlayer space of ReS_2 to form Na_xReS_2, and reduction of Na_xReS_2 into Na_2S and metallic Re by a conversion reaction, respectively. In the following anodic scan, a peak centered at 1.5 V is associated with the desodiation of Na_2S + Re composite into Li_xReS_2, followed by a distinct peak located at 2 V, which can be attributed to the formation of ReS_2.

Galvanostatic discharge-charge profiles of ReS_2/N-CNFs for the first three cycles at a current density of 100 mA/g between 0.01 and 3 V in NIBs are shown in Fig. 4b. The first discharge and charge capacities are 643 and 456 mA h/g, respectively, corresponding to CE of 70.9%, which is lower than that in LIBs, probably due to more reduction of electrolyte to form SEI in NIBs. In the following cycles, higher CE is obtained, reaching 92.3% in the third cycle, indicating highly reversible capacity. Besides, plateaus in the discharge-charge curves are in accordance with peaks in the CV. The cycling performance of ReS_2/N-CNFs in NIBs was measured at a current density of 100 mA/g between 0.01 and 3 V (Fig. 4c). ReS_2/N-CNFs shows a very stable long-term cycle life. The reversible capacity can maintain 300, 263, 245 mA h/g after 200, 400, and 800 cycles, respectively, with a slight decrease. Remarkably, the CE approaches above 99.5%, implying that superior cycle stability of ReS_2/N-CNFs electrode for reversible Na^+ storage was highly repeatable. In contrast, the capacity of pure ReS_2 falls dramatically to ~260 mA h/g within first 50 cycles, which shares the same trend with that in LIBs. Still, the cycling performance of N-CNFs for NIBs is investigated, which delivers a capacity of 204 mA h/ (Fig. S4c).

The CV of ReS_2/N-CNFs in KIBs was tested at a scan rate of 0.1 mV/s between 0.01 and 3 V (Fig. 4d). Based on the similar reaction mechanism with that in LIBs and NIBs, during the first cathodic cycle, ReS_2 hold K^+ within layers and then is reduced to metallic Re embedded in the matrix of K_2S. In the following anodic scan, Re and K_2S are oxidized to ReS_2.

Galvanostatic discharge-charge curves of ReS_2/N-CNFs for KIBs in the first three cycles at a current density of 50 mA/g between 0.01 and 3 V are shown in Fig. 4e. In the first cycle, discharge and charge capacity are 541, and 364 mA h/g, respectively, corresponding to CE of 67.3%. The CE of ReS_2/N-CNFs in the first cycle decreases from that in LIBs (73.9%), NIBs (70.9%), to KIBs (67.3%), which can be on account of different consumption of electrolyte on forming SEI and diverse electrochemical reversibility of alkali metal sulfide (Li_2S, Na_2S, and K_2S). Cycling performance of ReS_2/N-CNFs for KIBs was evaluated at a current density of 50 mA/g between 0.01 and 3 V (Fig. 4f). After 100 cycles, ReS_2/N-CNFs can obtain a discharge capacity of 253 mA h/g, superior to many reported anodes for KIBs [9,42,43]. Besides, CE of ReS_2/N-CNFs reaches 99% beyond the 5th cycle. In addition, ReS_2/N-CNFs tend to sustain the origin morphology even after 100 cycles in LIBs, NIBs, and KIBs (Fig. S5), indicating importance of flexible and tough N-doped CNFs to keep the structure intact. It is clear that SEI on the surface of ReS_2/N-CNFs is thicker after cycling in NIBs and KIBs than that in LIBs, which is in accordance with lower CE for the first cycle in NIBs and KIBs. By contrast, discharge capacity of pure ReS_2 drops sharply to below 200 mA h/g within 20 cycles, even though the capacity of N-CNFs can sustain 191 mA h/g after 100 cycles (Fig. S4c). Cycling deterioration of ReS_2/N-CNFs in KIBs compared to that in LIBs and NIBs could be attributed to more severe volume variation caused by conversion reaction and inferior electrochemical reversibility of K_2S.

To better understand the enhancement of N-CNFs to the electrochemical performance of ReS_2, electrochemical impedance spectra (EIS) of ReS_2/N-CNFs and pure ReS_2 before and after 100 cycles in LIBs, NIBs, and KIBs were carried out (Fig. 5). All the EIS are composed of a depressed semicircle in the high frequency region contributed by SEI resistance (R_{SEI}) and charge-transfer resistance (R_{ct}) and a sloping straight line in the low frequency region related with ion diffusion process called Warburg impedance. Comparing EIS of pristine ReS_2/N-CNFs and ReS_2 in LIBs (Fig. 5a), R_{ct} for ReS_2/N-CNFs is much smaller than that for pure ReS_2, indicating that N-doped CNFs contribute to the fast charge-transfer process. Meanwhile, R_{ct} and R_{SEI} of ReS_2/N-CNFs increase after cycling in LIBs, probably attributed to formation of stable SEI and a phase transformation during conversion reaction. The same trend can be observed in the EIS of ReS_2/N-CNFs and pure ReS_2 for NIBs and KIBs (Fig. 5b and c), which further confirms that N-doped CNFs contribute much to the improved electrochemical performance of ReS_2/N-CNFs in LIBs, NIBs, and KIBs. The flexible N-doped CNFs network can provide fast electron transfer and prohibit the intermediate products aggregated. In addition, the nitrogen doping in N-doped CNFs can absorb S and polysufide generated during conversion reaction to prevent them aggregated and dissolved in the electrolyte [31,32]. Furthermore, it can be clearly seen that R_{SEI} and R_{ct} of postcycled ReS_2/N-CNFs increase from in LIBs, NIBs to KIBs, which is in accordance with their

gradually reduced CE for the first cycle. It may be related with the different thickness of SEI layers, kinetics of various ion diffusing across SEI and in the active materials in LIBs, NIBs, and KIBs. To be specific, due to greater volume change of ReS_2/N-CNFs in KIBs, thicker SEI form on the surface of active materials. Meanwhile, because of larger K^+ diameter, it is more difficult for K^+ to cross the SEI layer in KIBs. Additionally, diffusion barrier of K^+ in active materials is higher than that in LIBs and NIBs. All of these reasons contribute to the greater R_{SEI} and R_{ct} in KIBs than that in LIBs and NIBs. More precise and deep analysis are under further investigation.

In summary, a universal anode based on the flexible ReS_2/N-CNFs-based paper was synthesized by a facile electrospinning and hydrothermal method and used as binder- and current collector-free anodes for alkali ion battery. ReS_2/N-CNFs take advantage of large interlayer spacing and extremely weakly van der Waals interaction of ReS_2, high conductivity and oriented electronic/ionic transport pathway of CNFs, and strong absorption of nitrogen doping to sulfur and polysulfide, thus showing excellent electrochemical performance in LIBs, NIBs, and KIBs. It exhibits reversible capacities of 440 mA h/g after 400 cycles at 100 mA/g in LIBs, 245 mA h/g after 800 cycles at 100 mA/g in NIBs, and 253 mA h/g after 100 cycles at 50 mA/g in KIBs, all of which are much better than that of pure ReS_2. Also, we firstly investigate the different electrochemical performance of ReS_2/N-CNFs in LIBs, NIBs, and KIBs. The results will hopefully intrigue more interests in ReS_2 used on energy storage and conversion.

Acknowledgments

This work was supported as part of the Nanostructures for Electrical Energy Storage (NEES), an Energy Frontier Research Center funded by the U.S. Department of Energy, Office of Science, Basic Energy Sciences under Award number DESC0001160. This work was also supported by the National Natural Science Foundation of China (Grant Nos. 51302079), Hunan Provincial Innovation Foundation for Postgraduate (no. CX2016B120). M. Mao's fellowship was supported by China Scholarship Council (grant no. 201606130050).

Notes

The authors declare no competing financial interest.

Appendix A. Supporting information

Supplementary data associated with this article can be found in the online version at http://dx.doi.org/10.1016/j.nanoen.2018.01.001.

References

[1] J.M. Tarascon, M. Armand, Nature 414 (2001) 359–367.
[2] M. Armand, J.M. Tarascon, Nature 451 (2008) 652–657.
[3] M.S. Whittingham, Chem. Rev. 104 (2004) 4271–4302.
[4] M.D. Slater, D. Kim, E. Lee, C.S. Johnson, Adv. Funct. Mater. 23 (2013) 947–958.
[5] H. Pan, Y.-S. Hu, L. Chen, Energy Environ. Sci. 6 (2013) 2338–2360.
[6] N. Yabuuchi, K. Kubota, M. Dahbi, S. Komaba, Chem. Rev. 114 (2014) 11636–11682.
[7] S.-W. Kim, D.-H. Seo, X. Ma, G. Ceder, K. Kang, Adv. Energy Mater. 2 (2012) 710–721.
[8] J. Zhao, X. Zou, Y. Zhu, Y. Xu, C. Wang, Adv. Funct. Mater. 26 (2016) 8103–8110.
[9] K. Share, A.P. Cohn, R. Carter, B. Rogers, C.L. Pint, ACS Nano 10 (2016) 9738–9744.
[10] W. Zhang, J. Mao, S. Li, Z. Chen, Z. Guo, J. Am. Chem. Soc. 139 (2017) 3316–3319.
[11] J.B. Goodenough, Y. Kim, Chem. Mater. 22 (2010) 587–603.
[12] M. Yoshio, H. Wang, K. Fukuda, Angew. Chem. 115 (2003) 4335–4338.
[13] D.A. Stevens, J.R. Dahn, J. Electrochem. Soc. 148 (2001) A803.
[14] W. Luo, J. Wan, B. Ozdemir, W. Bao, Y. Chen, J. Dai, H. Lin, Y. Xu, F. Gu, V. Barone, L. Hu, Nano Lett. 15 (2015) 7671–7677.
[15] S. Komaba, T. Hasegawa, M. Dahbi, K. Kubota, Electrochem. Commun. 60 (2015) 172–175.
[16] J. Xiao, D. Choi, L. Cosimbescu, P. Koech, J. Liu, J.P. Lemmon, Chem. Mater. 22 (2010) 4522–4524.
[17] C. Tan, X. Cao, X.-J. Wu, Q. He, J. Yang, X. Zhang, J. Chen, W. Zhao, S. Han, G.-H. Nam, M. Sindoro, H. Zhang, Chem. Rev. 117 (2017) 6225–6331.
[18] D. Wang, L.-M. Liu, S.-J. Zhao, Z.-Y. Hu, H. Liu, J. Phys. Chem. C 120 (2016) 4779–4788.
[19] S. Zhang, B.V.R. Chowdari, Z. Wen, J. Jin, J. Yang, ACS Nano 9 (2015) 12464–12472.
[20] E. Yang, H. Ji, Y. Jung, J. Phys. Chem. C 119 (2015) 26374–26380.
[21] J. Heo, H. Jeong, Y. Cho, J. Lee, K. Lee, S. Nam, E.-K. Lee, S. Lee, H. Lee, S. Hwang, S. Park, Nano Lett. 16 (2016) 6746–6754.
[22] D. Ovchinnikov, F. Gargiulo, A. Allain, D.J. Pasquier, D. Dumcenco, C.-H. Ho, O.V. Yazyev, A. Kis, Nat. Commun. 7 (2016) 12391.
[23] N.R. Pradhan, A. McCreary, D. Rhodes, Z. Lu, S. Feng, E. Manousakis, D. Smirnov, R. Namburu, M. Dubey, A.R. Hight Walker, H. Terrones, M. Terrones, V. Dobrosavljevic, L. Balicas, Nano Lett. 15 (2015) 8377–8384.
[24] X. Cao, Y. Shi, W. Shi, X. Rui, Q. Yan, J. Kong, H. Zhang, Small 9 (2013) 3433–3438.
[25] X. Wang, G. Li, M.H. Seo, F.M. Hassan, M.A. Hoque, Z. Chen, Adv. Energy Mater. 5 (2015) (n/a-n/a).
[26] S. Tongay, H. Sahin, C. Ko, A. Luce, W. Fan, K. Liu, J. Zhou, Y.-S. Huang, C.-H. Ho, J. Yan, D.F. Ogletree, S. Aloni, J. Ji, S. Li, J. Li, F.M. Peeters, J. Wu, Nat. Commun. 5 (2014) 3252.
[27] J. Gao, L. Li, J. Tan, H. Sun, B. Li, J.C. Idrobo, C.V. Singh, T.-M. Lu, N. Koratkar, Nano Lett. 16 (2016) 3780–3787.
[28] Q. Zhang, S. Tan, R.G. Mendes, Z. Sun, Y. Chen, X. Kong, Y. Xue, M.H. Rümmeli, X. Wu, S. Chen, L. Fu, Adv. Mater. 28 (2016) 2616–2623.
[29] F. Qi, J. He, Y. Chen, B. Zheng, Q. Li, X. Wang, B. Yu, J. Lin, J. Zhou, P. Li, W. Zhang, Y. Li, Chem. Eng. J. 315 (2017) 10–17.
[30] F. Qi, Y. Chen, B. Zheng, J. He, Q. Li, X. Wang, J. Lin, J. Zhou, B. Yu, P. Li, W. Zhang, Appl. Surf. Sci. 413 (2017) 123–128.
[31] J. Song, T. Xu, M.L. Gordin, P. Zhu, D. Lv, Y.-B. Jiang, Y. Chen, Y. Duan, D. Wang, Adv. Funct. Mater. 24 (2014) 1243–1250.
[32] J. Song, M.L. Gordin, T. Xu, S. Chen, Z. Yu, H. Sohn, J. Lu, Y. Ren, Y. Duan, D. Wang, Angew. Chem. Int. Ed. 54 (2015) 4325–4329.
[33] M. Mao, F. Yan, C. Cui, J. Ma, M. Zhang, T. Wang, C. Wang, Nano Lett. 17 (2017) 3830–3836.
[34] L. Wu, T. Wu, M. Mao, M. Zhang, T. Wang, Electrochim. Acta 194 (2016) 357–366.
[35] J.P. Zhao, Z.Y. Chen, T. Yano, T. Ooie, M. Yoneda, J. Sakakibara, J. Appl. Phys. 89 (2001) 1634–1640.
[36] P. Hammer, N.M. Victoria, F. Alvarez, J. Vac. Sci. Technol. A: Vac. Surf. Films 18 (2000) 2277–2287.
[37] J. Yu, M. Guo, F. Muhammad, A. Wang, F. Zhang, Q. Li, G. Zhu, Carbon 69 (2014) 502–514.
[38] J.W. Jang, C.E. Lee, S.C. Lyu, T.J. Lee, C.J. Lee, Appl. Phys. Lett. 84 (2004) 2877–2879.
[39] F. Qi, Y. Chen, B. Zheng, J. He, Q. Li, X. Wang, B. Yu, J. Lin, J. Zhou, P. Li, W. Zhang, J. Mater. Sci. 52 (2017) 3622–3629.
[40] K. Chang, W. Chen, ACS Nano 5 (2011) 4720–4728.
[41] M. Mao, L. Mei, D. Guo, L. Wu, D. Zhang, Q. Li, T. Wang, Nanoscale 6 (2014) 12350–12353.
[42] Z. Jian, Z. Xing, C. Bommier, Z. Li, X. Ji, Adv. Energy Mater. 6 (2016) (n/a-n/a).
[43] I. Sultana, T. Ramireddy, M.M. Rahman, Y. Chen, A.M. Glushenkov, Chem. Commun. 52 (2016) 9279–9282.

Minglei Mao is currently a Ph.D. candidate at College of Chemistry and Chemical Engineering, Hunan University. He received his bachelor degree from College of Materials Science and Engineering, Hunan University. His research interests focus on the development of electrode materials to improve the performance of LIBs, NIBs, and KIBs.

Chunyu Cui received his bachelor degree, and is currently a Ph.D. candidate, at College of Chemistry and Chemical Engineering, Hunan University. His research interests are design of materials structure to achieve the high performance of LIBs and NIBs.

Mingguang Wu is current undertaking his Master degree at School of Physics and Electronics, Hunan University. His research interests are electrocatalysis for oxygen reduction reaction.

Dr. Ming Zhang is an associate professor in Hunan University. He has published more than 70 papers. His research is focused on the synthesis of carbon-based nanocomposites and their application in LIBs and NIBs.

Dr. Tao Gao received his bachelor degree in Automotive Engineering and M.S. degree in Mechanical Engineering both from Tsinghua University, and Ph.D. degree in Chemical Engineering from University of Maryland. His research interest is chemistry and system innovation for next generation batteries and electrochemical methods.

Dr. Xiulin Fan received his bachelor degree and Ph.D. degree both in Materials Science and Engineering from Zhejiang University. He is currently an assistant research scientist at University of Maryland-College Park. His research interests are novel materials and their application in energy storage and conversion devices including lithium-ion batteries, sodium-ion batteries and hydrogen storage. He has more than 80 peer-reviewed journal publications.

Dr. Ji Chen received his bachelor and Ph.D. degree from Department of Chemistry, Tsinghua University. He is currently a postdoctoral research associate at University of Maryland, College Park. His research interests are all solid-state Li-ion batteries.

Prof. Taihong Wang is a Cheung Kong Professor in Hunan University since 2005. His research interests include ultrasensors, lithium ion batteries, and nanodevices. He has published more than 200 papers, and more than 80 papers were published in the noted Journal of Applied Physics Letters in the field of applied physics. More than 50 items of his patents have been authorized.

Dr. Jianmin Ma is an Associate Professor at Hunan University, China. He received his B.Sc. degree in Chemistry from Shanxi Normal University in 2003 and Ph.D. degree in Materials Physics and Chemistry from Nankai University in 2011. During 2011–2015, he also conducted research in several overseas universities as a postdoctoral research associate. His research interests focus on the synthesis of nanostructured materials, electrochemical storage devices, electrocatalysis, and gas sensors.

Prof. Chunsheng Wang is a full professor at University of Maryland College Park (UMCP). He was educated in materials science and trained in electrochemistry, and got his Ph.D. degree from Zhejiang University. He has more than 150 peer-reviewed journal publications and more than 25 years of experience in battery research. His Li ion battery research has been highlighted in EFRC news by DoE in 2012, and by Chemical & Engineering News in 2013. He is a recipient of the University of Maryland Outstanding junior Researcher Award.